JOURNAL OF SOLID STATE CHEMISTRY 36, 97–106 (1981)

Structural Aspects of the Metal–Metal Interactions in the $Ti_{1+x}S_2$ Materials

E. TRONC AND R. MORET*

Laboratoire de Chimie Appliquée de l'Etat Solide,† ENSCP, 11 rue Pierre et Marie Curie, 75231 Paris Cédex 05, France

Received December 19, 1979; in revised form March 31, 1980

Interlayer metallic interactions are shown to manifest themselves in both stacking correlations and titanium sublattice distortions. A quantitative study is reported through the structure refinement of one of the $Ti_{1.33}S_2$ superstructures. The interactions seem to involve Coulomb repulsion forces and should be valid in a broad composition range. Lattice distortions are predicted for other structures including the nonstoichiometric 1*T* structure.

Introduction

Deviations from the ideal structure are known to act on the electronic properties of TiS_2 (*1*) which are now understood through improved band calculations (*2, 3*) and structural defect models. These models involve a transfer of Ti atoms from the filled sandwiches into the van der Waals gap sites (*4*) and, among others, they raise the question of Ti–Ti interactions.

In the TiS_2–TiS range, the Ti–Ti interactions take several forms. For high metal contents ($Ti_{1.5}S_2$–TiS range) the occupancy of successive titanium layers appears to follow a concentration wave model in the c direction (*5*). In the TiS_2–$Ti_{1.5}S_2$ region the metal layers are successively fully and partly occupied. Around $Ti_{1.20}S_2$, diffuse scattering experiments have shown that the Ti atoms are partially ordered in the defective layers (*6*). Moreover, in the same region, a number of different sulfur layer stackings (polytypes) have been observed (*7, 8*). The role of the partially ordered Ti atoms is here particularly striking since the stacking faults which are involved in the growing mechanisms proposed for these polytypes are predominantly located in the defective layers (*9, 10*).

The titanium partial order is mainly two dimensional around $Ti_{1.20}S_2$ although occupancy correlations between defective layers have been observed (*6*). As the titanium concentration x ($Ti_{1+x}S_2$) increases and reaches $x = \frac{1}{3}$, a 2D superstructure forms. Furthermore, for the same composition, the interlayer correlations tend to induce long-range ordering, sometimes producing 3D superstructures of the 4H basic structure, as is described in the next section. These superstructures are particularly appropriate for the study of another type of Ti–Ti interactions, namely, distortions within the metallic sublattice. Such distor-

* Present address: Physics Department, Purdue University, West Lafayette, Ind. 47907.

† Laboratoire Associé au CNRS No. 302.

0022-4596/81/010097-10$02.00/0

tions have already been studied to a certain extent (*8, 11*) and the main purpose of this work is to show that the situation is more complex and informative than previously acknowledged.

Coulomb repulsion seems to be the common driving phenomenon lying behind the Ti–Ti interactions. In that respect the results we report here should apply to the whole TiS_2–TiS diagram and, for instance, they could be used to clarify the TiS_2 case.

Stacking Correlations between Partly Occupied Titanium Layers

The $Ti_{1.33}S_2$ superstructures derive from the 4H model (a_0, c_0) (Fig. 1) by titanium ordering within and between the defective layers. In these layers, in accordance with the Ti concentration ($x = \frac{1}{3}$), every second-nearest-neighbor site is occupied, leading to the ($a_0 3^{1/2} \times a_0 3^{1/2}$) 2D superstructure. Given a defective layer, the successive equivalent layer can be deduced by one of the three possible translations $\mathbf{a}_0 + \mathbf{c}_0$, $\mathbf{c}_0$, $-\mathbf{a}_0 + \mathbf{c}_0$ so that stacking correlations, if strong enough, may produce various arrangements along the c_0 direction. Different stages, varying from long-range to short-range order, have been observed for single crystals grown by the vapor transport method and belonging to the same preparation tube.

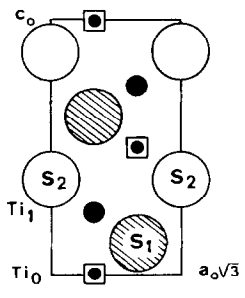

FIG. 1. (11.0) section of the 4H basic structure. Ti_0 and Ti_1 stand for atoms of the partly and fully occupied layers, respectively.

$Ti_{1.33}S_2$ Superstructures

Two superstructures have been observed:

—$4H_2$ ($a_0 3^{1/2} \times a_0 3^{1/2} \times 2c_0$) has already been studied by Bartram (*12*) and was recently observed by high-resolution electron microscopy (*13*).

—$4H_3$ ($a_0 3^{1/2} \times a_0 3^{1/2} \times 3c_0$) has been reported recently (*14*) and probably corresponds to the $Ti_{1.50}S_2$ structure mentioned in (*13*) (see also the Appendix).

The identification of the defective layer stackings has been achieved from the examination of the diffraction patterns (Figs. 2a, b). Let us call B_i and C_i (i = 1, 2, or 3) the possible B and C sites of the 2D $Ti_{1.33}S_2$ supercell (Fig. 3), and label the defective layers according to their occupied sites. Then, the stacking sequence of the defective layers in the substructure and the two superstructures can be written as follows:

4H $\cdots C/BC/B \cdots$,

$4H_2$ $\cdots C_2/B_1C_1B_2C_2/B_1 \cdots$,

$4H_3$ $\cdots C_3/B_1C_1B_2C_2B_3C_3/B_1 \cdots$.

The stacking lowers the symmetry from $P6_3mc$ (4H) to Cc in both cases, and induces a domain structure characterized by six orientation variants, according to the ratio of the point group orders 12 (6*mm*) and 2 (*m*). Though nonconventional, the hexagonal superstructure unit cell will be used hereafter. Connection with the Cc nonprimitive unit cell is given in Table I.

Assuming (i) a mosaic-block-like behavior of the domains with respect to diffraction, (ii) equal amounts of each variant, and (iii) equidistant layers, we obtain a simple intensity model for the superstructure reflections. All reciprocal rows (along $\mathbf{c}^*$) are identical and the reflection intensities can be written

$$4H_2: \quad I(l) = 4f_{Ti}^2 [1 + \cos 2\pi(\tfrac{1}{3} + l/2)]$$

two types of reflections alternate:

$$l = 2n, \qquad I(l) = 2f_{Ti}^2,$$
$$l = 2n + 1, \qquad I(l) = 6f_{Ti}^2.$$

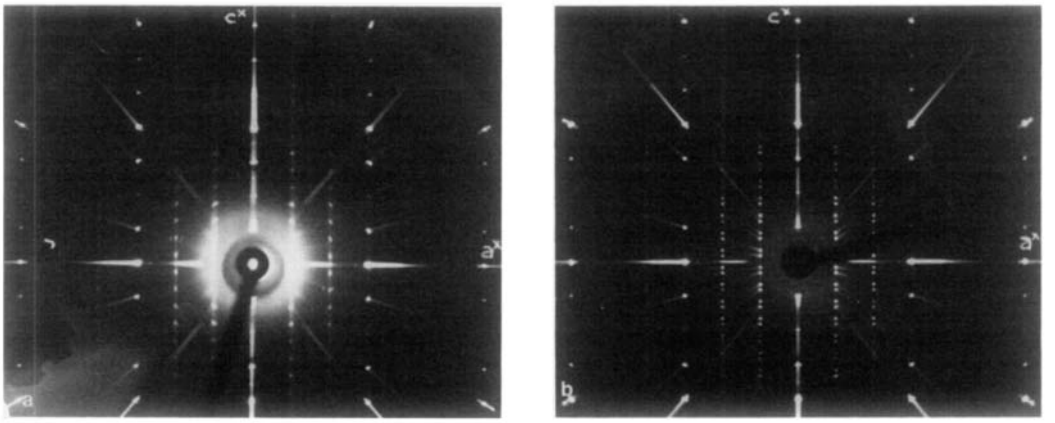

FIG. 2. X-Ray precession photographs of $Ti_{1.33}S_2$ superstructures (a) $4H_2$, (b) $4H_3$.

$$4H_3: \quad I(l) = 18f_{Ti}^2[1 - \cos 2\pi l/3]$$

The intensity distribution here is the same as that for rhombohedral twins,

$$l = 3n, \qquad I(l) = 0,$$
$$l = 3n \pm 1, \qquad I(l) = 27f_{Ti}^2,$$

where f_{Ti} is the titanium scattering factor. These intensity distributions provide a fairly good qualitative description of the diffraction patterns (Figs. 2a, b).

Stacking Faults

In both structures, it is worth pointing out that successive B (C) layers are related by translations of the type $\pm\mathbf{a}_0 + \mathbf{c}_0$ (and not $\mathbf{c}_0$). Therefore each "B (C) sublattice" generated by these layers satisfies a sort of close-packing condition. However, stacking faults which fulfill this condition but break the superlattice periodicity must have little influence on the Coulomb interaction energy. Such faults are thus expected to form easily.

This is in agreement with the observation of diffuse streaks along the superstructure rows on the diffraction patterns (see Fig. 2a). These streaks have been observed frequently and for some crystals the superstructure peaks even disappear. In this case the streaks still exhibit broad intensity maxima equally spaced along the rows, and it can be shown (*15*) that such an intensity modulation corresponds to a completely disordered close-packed stacking of hexagonal layers.

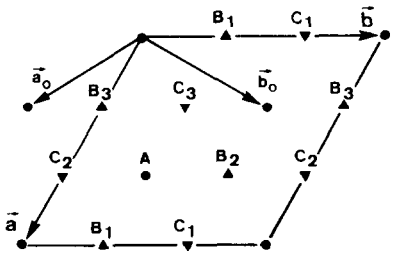

FIG. 3. Two-dimensional representation of the various sites in the $Ti_{1.33}S_2$ superstructures.

Titanium Sublattice Distortions in the $4H_3$ Superstructure

A close examination of the diffraction patterns (Figs. 2a, b) reveals that the superstructure reflections do not exactly follow the simple distributions given above. Such relations as

$$I(10.9) \simeq I(10.11) < I(10.13) \qquad (4H_2, \text{ Fig. 2a}),$$
$$I(\bar{1}0.17) < I(\bar{1}0.20) > I(\bar{1}0.23) \qquad (4H_3, \text{ Fig. 2b})$$

are the signature of deviations from the

TABLE I

$4H_3$ SUPERSTRUCTURE UNIT CELL

	Hexagonal description		Monoclinic description
Unit cell	$\mathbf{a} = 2\mathbf{a}_0 + \mathbf{b}_0$	$a = 5.949(1)$ Å	$\mathbf{a}' = \mathbf{a} - \mathbf{b}$
	$\mathbf{b} = -\mathbf{a}_0 + \mathbf{b}_0$		$\mathbf{c}' = \mathbf{a} + \mathbf{b}$
	$\mathbf{c} = 3\mathbf{c}_0$	$c = 34.385(6)$ Å	
	Coordinates of equivalent positions		
Rhombohedral stacking	$(0, 0, 0; \frac{2}{3}, \frac{1}{3}, \frac{1}{3}; \frac{1}{3}, \frac{2}{3}, \frac{2}{3})$		$(0, 0, 0; \frac{2}{3}, 0, \frac{1}{3}; \frac{1}{3}, 0, \frac{2}{3})$
Cc space group	$+ x, y, z; \bar{y}, x, \frac{1}{2} + z$		$+ (0, 0, 0; \frac{1}{2}, \frac{1}{2}, 0)$
			$+ x, y, z; x, \bar{y}, \frac{1}{2} + z$

ideal model in the form of a corrugation of the completely filled Ti layers. The details of the implicated distortions have been obtained from the refinement of the $4H_3$ superstructure, as we describe now.

Data Collection

Mo$K\alpha$ radiation was chosen in order to obtain an accurate determination of the distortions. Owing to the large number of reflections (about 10^5 independent ones), intensity measurements have been limited to reciprocal rows parallel to $\mathbf{c}^*$, with:

(i) a short projection of the scattering vector $\mathbf{s}$ ($|\mathbf{s}_{hk.0}| < 7^{1/2}a^*$) for the superstructure rows since in-plane shifts were thought to be much smaller than out-of plane ones,

(ii) a longer projection ($|\mathbf{s}_{hk.0}| < (147)^{1/2}a^*$) for the basic rows in order to check the above-mentioned assumption.

Data were collected on a three-circle diffractometer. The crystal, a nearly hexagonal platelet ($0.31 \times 0.29 \times 0.04$ mm), was mounted along $\mathbf{a}_0^*$. Two thousand four hundred nine independent reflections were measured: 1167 reliable ones ($I > 4\sigma(I)$) were retained and corrected for Lorentz-polarization effects. Rough absorption corrections ($\mu = 61$ cm^{-1}), necessarily neglecting the domain structure, were performed by the Gaussian numerical method. Structure refinements were separately performed on basic and superstructure reflections. No weight coefficients were used. Atomic scattering factors were taken from (*16*).

Solution to the Domain Structure

The orientation variants involved are related by the symmetry elements discarded by the ordering: threefold axis and a mirror plane of the (10.0) type in the basic structure. We assume that the domains have a mosaic-block-like behavior so that the intensity $I(hk.l)$ scattered at the $hk.l$ reciprocal point can be written as

$$I(hk.l) = \sum_{i=1}^{6} k_i |F_i(hk.l)|^2,$$

where k_i is a scale factor relative to variant i and F_i $(hk.l)$ is the corresponding structure factor. Least-squares refinement can still be performed if the minimized quantity is $\Sigma(I_{obs} - |I_{calc}|)^2$ and not, as is more usual, $\Sigma(F_{obs} - |F_{calc}|)^2$.

Since the substructure reflections obey relations of the type I_{obs} $(hk.l)$ = I_{obs} $(kh.l)$ = I_{obs} $(hk.\bar{l})$, it is considered that (x, y) shifts are negligible. Then, all variants contribute equally to these reflections (except for their scale factors).

Furthermore, for each rhombohedral orientation, at most three variants contribute to a given superstructure reflection. It can be shown that refinements of the domain

structure can be performed since the intensities can be expressed as

$$I\ (hk.l) = K_j|F_1\ (hk.l)|^2,$$

where $F_1\ (hk.l)$ is the structure factor for a reference variant and K_j is one out of five possible linear combinations of the scale factors k_i.

Structure Refinement

Space group requirements plus the rhombohedral stacking condition theoretically lead to 10 independent atoms: one layer of each type (S_1, S_2, Ti_1, Ti_0) (Fig. 1) is involved in the supercell, with 3 independent atoms per compact layer and 1 in the defective layer which we can fix on the z-axis origin. Coordinates of equivalent positions are given in Table I. For reasons mentioned above, (x, y) variations were neglected and z displacements alone taken into account.

Basic reflections are but slightly altered by the expected wrinkling of the layers. At this stage, this effect has been neglected so that the average position of the layers has been obtained. The refinement of nine parameters (one scale factor, one z coordinate per compact layer, four isotropic temperature factors, and the defective layer occupancy coefficient) performed on 197 independent reflections leads to a reliability index R ($R = \Sigma\ |F_{obs} - |F_{calc}|\ |/\Sigma\ F_{obs}$) equal to 0.025. Atomic parameters are given in Table IIA. The derived composition is $Ti_{1.335}S_2$, which is identical, within the standard deviation, to the ideal composition.

Further refinements were performed on 250 independent superstructure reflections ($-h + k + l = 3n$). Temperature factors were fixed at their values given in Table IIA. Unsplit fully occupied layers do not contribute to superstructure reflections which, in the average superstructure approximation, are thus only due to the Ti_0 atoms. Introduction of five scale factors therefore provides a direct test for the validity of the domain structure refinement procedure. Such a model converged to $R = 0.11$. In the next step, corrugation of the Ti_1 layer was introduced (with a constraint on the displacements according to the symmetry imposed by the neighboring Ti_0 site occupation and on the layer average position) and the R value decreased by 0.02.

TABLE II

ATOMIC PARAMETERS FOR THE $4H_3$ SUPERSTRUCTURE[a]

A. Average superstructure[b]					B. Final parameters[c]				
Layer	Site type	Occupancy coefficient	z	B (Å²)	Atom	Multiplier[d]	x	y	z
Ti_0	B	1.004 (15)	0	0.417(30)	Ti_0	1	0	$\frac{1}{3}$	0
Ti_1	B	3	0.08851(6)	0.576(8)	Ti_{11}	1	0	$\frac{1}{3}$	0.08925(8)
					Ti_{12}	2	$\frac{1}{3}$	0	0.08814(8)
S_1	C	3	0.04593(6)	0.494(14)	S_{11}	1	0	$\frac{2}{3}$	0.04667(9)
					S_{12}	2	$\frac{2}{3}$	0	0.04556(9)
S_2	A	3	0.13062(6)	0.549(14)					

[a] Standard deviations given in parentheses.

[b] Basic reflections fit.

[c] Superstructure reflections fit. The B's and Ti_1 and S_1 layer average positions are fixed at their values in Table IIA.

[d] In accordance with the local symmetry of a TiS_2 sandwich plus its adjacent Ti_0 layers.

Improvement of the fit (decrease of about 0.015) was then reached by considering a distortion of the S_1 layer. On the other hand, no evidence for a similar effect was obtained for the S_2 layer. Refinement of seven parameters (five scale factors and two positional parameters) thus converged to $R = 0.073$. The lifting of all constraints (including the layer average positions) did not prove significant. Atomic parameters are given in Table IIB.

From the scale factor analysis, the variant relative contributions to the scattered intensity have been deduced. They approximately range from 1 to 4.8, both rhombohedral stacking orientations being nearly equally represented.

In the course of the refinements we found that the data seem to favor Ti^{4+} rather than Ti for the atomic scattering factor of Ti_1. On the other hand, no preference was detected for Ti_0. The significance of this result is questionable, because of the high correlation with the temperature factors and of the small R decrease implied (about 0.004). However, this indication is consistent with the delocalization of the d electrons of the Ti atoms, which is widely accepted (*1*).

Further improvement of the fit is actually hindered by the complex domain structure and the overall low intensity of the superstructure reflections. Nevertheless, the main features of the distortions are clearly established.

No quantitative refinement has been performed on the $4H_2$ superstructure. Similar distortions should exist here. From a simple calculation one can show that they give a qualitative account of the superstructure intensity distribution (Fig. 2a).

Description of the Distortions

Each titanium atom is surrounded by a distorted octahedron of sulfur atoms. Around a sulfur atom, the Ti_1 and Ti_0 sites form either an octahedron (S_2 atom) or a trigonal prism (S_1 atom). In the latter configuration, two situations arise for a Ti_1 atom, depending on whether the nearest-neighbor interstitial site is occupied or not. It corresponds to the Ti_{11} and Ti_{12} atoms, respectively. See Fig. 4 where comparison with the 4H (*11*) and 1*T* (*17*) situations so far acknowledged is also made. The compact layer corrugation is clearly related to the Ti_{11}-type configuration. Interatomic distances are given in Table III.

The $4H_3$ superstructure can be described as a stacking of six TiS_2 sandwiches regularly shifted and twisted around the pinning

TABLE III

INTERATOMIC DISTANCES IN THE $4H_3$ SUPERSTRUCTURE

	Distance (Å)	Angle[a] (°)
Ti_{11}–Ti_0	3.069(4)	
Ti_{11}–Ti_0	3.320(3)	
Ti_{11}–S_{11}	2.465(3)	53.57(4)
Ti_{11}–S_{12}	2.488(3)	52.86(4)
Ti_{11}–S_2	2.441(3)	54.34(5)
S_{11}–S_2	3.502(4)	
S_{12}–S_2	3.533(4)	
Ti_{12}–Ti_0	3.350(3)	
Ti_{12}–S_{11}	2.443(3)	54.28(4)
Ti_{12}–S_{12}	2.465(3)	53.55(4)
Ti_{12}–S_2	2.463(3)	53.63(5)
S_{11}–S_2	3.502(4)	
S_{12}–S_2	3.533(4)	
Ti_0–S_{11}	2.551(3)	51.02(4)
Ti_0–S_{12}	2.527(3)	51.69(4)
Ti_0–S_2	2.339(2)	57.99(5)
S_{11}–S_2	3.467(4)	
S_{12}–S_2	3.436(4)	
Ti_0–Ti_0	5.949(1)	
Ti_{11}–Ti_{11}	5.949(1)	
Ti_{12}–Ti_{12}	3.435(1)	
Ti_{11}–Ti_{12}	3.435(1)	
S_{11}–S_{11}	5.949(1)	
S_{12}–S_{12}	3.435(1)	
S_{11}–S_{12}	3.435(1)	
S_2–S_2	3.435(1)	

[a] Between the corresponding bond and the c direction.

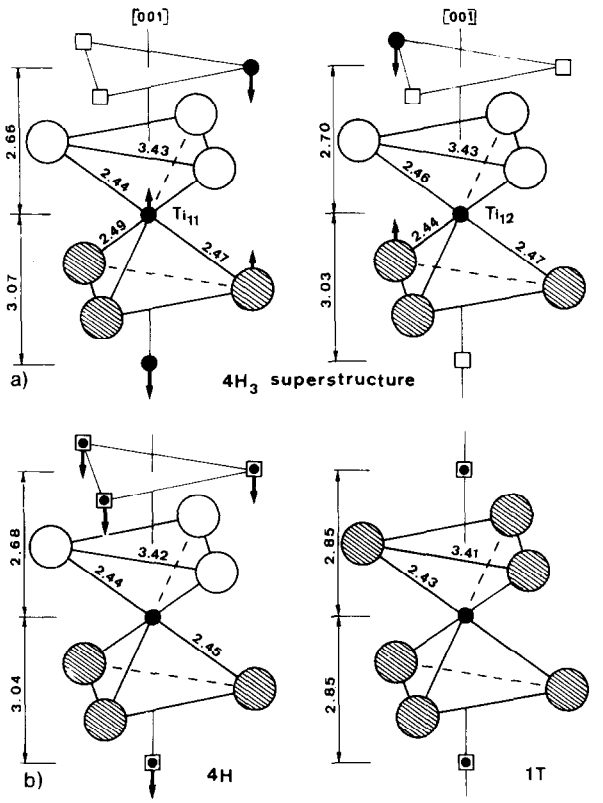

FIG. 4. Distortions in the $4H_3$ superstructure (a), and comparison with 4H (*11*) and 1*T* (*18*) structures (b). Ti atoms are represented by black circles, vacancies by open squares. Other symbols have the same meanings as in Fig. 1.

interstitial atoms. These extra atoms array themselves on parallel zig-zag chains all through the structure and directly induce a wrinkling in the TiS_2 sandwiches (Fig. 5). Similar features apply to the $4H_2$ superstructure.

The metal sublattice distortions can be decomposed into two parts. For the equidistant layer model, octahedral (around S_2) and trigonal prismatic (around S_1) configurations of Ti atoms would result in very different Ti–Ti distances: 3.48 and 2.86 Å, respectively. Relaxation of the latter actually occurs through:

A shift of the partly occupied layers. The (Ti_0–Ti_1) layer spacing is equal to 3.04 Å. It corresponds to a 6% (0.18 Å) increase in the "prismatic" distance. A similar situation has been found in 4H (*11*) and 12*R* (*8*) structures. This behavior is presumably general and we think it should occur within

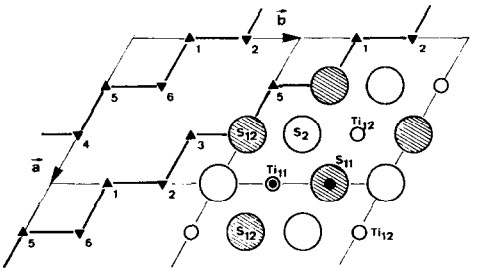

FIG. 5. Schematic representation of the $4H_3$ superstructure. Projection on the (00.1) plane of one-sixth of the unit cell content is drawn on the right side. Black circles stand for Ti_0 atoms (0, $\frac{1}{3}$, 0; 0, $\frac{2}{3}$, $\frac{1}{6}$). Ti_0 atom successive locations are given on the left side.

a broad composition range in the TiS_2–TiS system.

Corrugation of the fully occupied layers. The true "prismatic" distance is in fact about 1% longer, and equal to 3.07 Å. The layer splitting is equal to 0.04 Å. It suggests that the Coulomb repulsion is strong enough to overcome the atomic close-packing cohesion forces. The S_1 sublattice distortions (S_1 and Ti_1 layer splittings are found equal) probably help to stabilize the distorted octahedron around the Ti_{11} atom, possibly through a decrease of the Ti_{12} atom coordination unit energy.

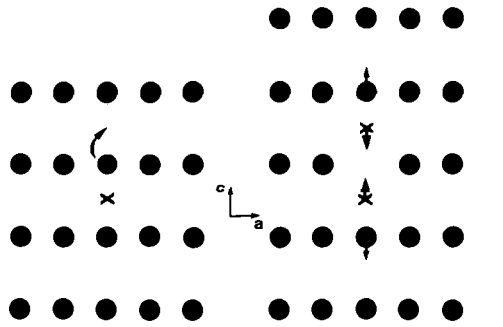

FIG. 7. Structural defect model for the 1*T* $Ti_{1+x}S_2$ structure. (10.0) section. Crosses stand for interstitial atoms.

Discussion

The Ti_0–Ti_{11} distance stretching described above is the most important of our results. This effect is probably independent of the 2D Ti_0 atom ordering and of the particular stacking of the $4H_2$ and $4H_3$ superstructures. Moreover, the Ti_1 layer splitting strongly supports the consideration of Ti–Ti *pair* interaction which implies a weak dependence on the titanium concentration, especially in the TiS_2–$Ti_{1.5}S_2$ range. Therefore it is likely that whenever two Ti atoms are related by a translation of the type $c_0/2$ (referred to the TiS_2 unit cell), Ti sublattice distortions will occur and the interatomic distance will be close to 3.07 Å. We briefly outline this situation for the common structures 4H, 12*R*, and 1*T*.

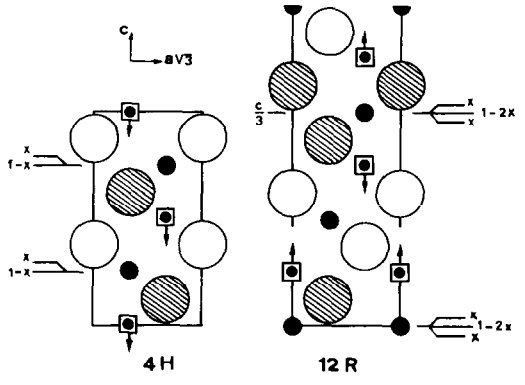

FIG. 6. Metal sublattice distortions in 4H and 12*R* $Ti_{1+x}S_2$ structures. Symbols have the same meanings as in Fig. 1.

4H and 12*R* previous refinements (*8*, *11*) took account only of the defective layer shifts. Direct application of our findings leads to the Ti filled layer splittings schematically represented in Fig. 6. In the 12*R* structure the filled layers are symmetrically surrounded by the defective ones and at first sight no wrinkling should occur. However, the preceding arguments lead to a threefold splitting of every other filled layer although the average position remains the same. Such a model for the distortions requires that identical sites in the neighboring defective layers be not simultaneously occupied.

In the 1*T* nonstoichiometric structure, all interlayer metal–metal bonds are of the "prismatic" type and the displacements along c of atoms inserted in the van der Waals gap are locked. However, the Ti–Ti repulsion should still occur and we suggest the following defect model for its relaxation. Occupation of a van der Waals site might induce the transfer of one Ti atom from one of the adjacent filled layers into its other neighboring van der Waals site (this is the defect model postulated to account for the transport properties of TiS_2 (*1*, *4*)). Re-

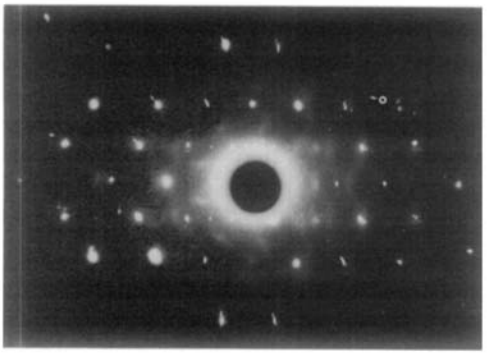

FIG. 8. X-Ray diffuse scattering pattern of $1T$ $Ti_{1+x}S_2$.

laxation could then occur through displacement of both atoms toward the created vacancy (Fig. 7).

As suggested earlier (*1*), the streaks observed on electron (*18*) and X-ray (Fig. 8) diffuse scattering patterns might be due to local ordering of these defects. It is worth noting that the complex array of streaks visible in Fig. 8, although not clarified, implies that correlations in the defect short-range ordering occur along **c**.

As a final comment, we would like to point out the possible relationship between the Ti–Ti repulsion that we have observed here and (i) the relatively narrow composition range of the $1T$ phase, (ii) the structural complexity of the Ti–S system compared, for instance, with the situation in the Ti–Se and Ti–Te systems.

Appendix

Two papers dealing with the same superstructures have been published very recently (*19*). The authors report studies by powder X-ray diffraction and high-resolution electron microscopy. As far as the Ti defective layer stackings are concerned there is agreement between our results and theirs. However, a few comments should be made. Because of the possible composition fluctuations in the same preparation and eventually in the same crystal, it is questionable to assert, as the authors do, that there is a definite relationship between composition and defective layer stacking.

The equidistant layer model is used by the authors for the refinement of the powder diffraction intensities. In that respect a single-crystal study proves to be much more informative.

Finally, one notes some discrepancies in cell parameters between the two works (especially for the **c** axis), which might be related to the stacking fault problem.

Acknowledgment

We should like to express our thanks to M. Huber for helpful comments.

References

1. J. A. WILSON, *Phys. Status. Solidi. B* **86,** 11 (1978).
2. A. ZUNGER AND A. J. FREEMAN, *Phys. Rev. B* **16,** 906 (1977).
3. J. V. MCCANNY, *J. Phys. C* **12,** 3263 (1979).
4. S. TAKEUCHI AND H. KATSUTA, *J. Japan Inst. Met.* **34,** 758 (1970).
5. G. A. WIEGERS AND F. JELLINEK, *J. Solid State Chem.* **1,** 519 (1970).
6. R. MORET, E. TRONC, M. HUBER, AND R. COMES, *Phil. Mag. B* **38,** 105 (1978).
7. E. TRONC AND M. HUBER, *J. Phys. Chem. Solids* **34,** 2045 (1973).
8. E. TRONC, R. MORET, J. J. LEGENDRE, AND M. HUBER, *Acta Crystallogr. Sect. B* **31,** 2800 (1975).
9. J. J. LEGENDRE, R. MORET, E. TRONC, AND M. HUBER, *J. Appl. Crystallogr.* **8,** 603 (1975).
10. J. J. LEGENDRE AND M. HUBER, *Acta Crystallogr. Sect. A* **33,** 971 (1977).
11. L. J. NORRBY AND H. FRANZEN, *J. Solid State Chem.* **2,** 519 (1970).
12. S. F. BARTRAM, Ph.D. thesis, Rutgers University, New Brunswick, N.J. (1958).
13. Y. BANDO, M. SAEKI, Y. SEKIKAWA, Y. MATSUI, S. HORIUCHI, AND M. NAKAHIRA, *Acta Crystallogr. Sect. A* **35,** 564 (1979).

14. E. TRONC AND R. MORET, 6th International Conference on Solid Compounds of Transition Elements, Stuttgart (1979).

15. A. GUINIER, "Théorie et technique de la radiocristallographie," Dunod, Paris (1964).

16. D. T. CROMER AND J. T. WABER, "International Tables for X-Ray Crystallography," Vol. IV, Kynock Press, Birmingham.

17. A. H. THOMPSON, F. R. GAMBLE, AND C. R. SYMON, *Mater. Res. Bull.* **10,** 915 (1975).

18. J. A. WILSON, F. J. DI SALVO, AND S. MAHAJAN, *Advan. Phys.* **24,** 117 (1975).

19. M. ONODA, M. SAEKI, AND I. KAWADA, *Z. Anorg. Allg. Chem.* **457,** 62 (1979); Y. BANDO, M. SAEKI, M. ONODA, I. KAWADA, AND M. NAKAHIRA, *Acta Crystallogr. Sect. B* **35,** 2522 (1979).